Letter

Anomalous Hall effect by chiral spin textures in the two-dimensional Luttinger model

Ryunosuke Terasawa and Hiroaki Ishizuka
Department of Physics, Tokyo Institute of Technology, Meguro, Tokyo 152-8551, Japan

(Received 30 September 2023; revised 22 December 2023; accepted 17 January 2024; published 22 February 2024)

Long-range magnetic textures, such as magnetic skyrmions, give rise to rich transport properties in magnetic metals, such as the anomalous Hall effect related to spin chirality, aka topological Hall effect. In addition to the topological Hall effect, recent studies on *noncentrosymmetric* magnets have found that the spin-orbit interaction of itinerant electrons gives rise to unique contributions related to spin chirality, i.e., the chiral Hall effect. In this paper, we discuss that the spin-orbit interaction has a distinct yet significant effect on the anomalous Hall effect related to spin chirality in *centrosymmetric* magnets. Using a scattering theory method, we find that the anomalous Hall effect related to scalar spin chirality in a two-dimensional Luttinger model is suppressed by more than one order of magnitude compared to the quadratic dispersion, and the contributions similar to the chiral Hall effect in Rashba models vanishes. At the same time, a unique term related to vector spin chirality occurs, which gives different Hall conductivities for the Bloch and Neel skyrmions, thereby enabling detection of the skyrmion helicity. The striking differences demonstrate the rich effect of crystal symmetry on the chirality-related anomalous Hall effect in materials with strong spin-orbit interactions.

DOI: 10.1103/PhysRevB.109.L060407

Introduction. Noncollinear magnetic textures give rise to rich transport phenomena, such as anomalous [1–7] and spin [8,9] Hall effects, and electrical magnetochiral effect [10–12]. Theoretically, these phenomena are often related to spin chirality: the anomalous Hall effect (AHE) is related to scalar spin chirality of three spins $\boldsymbol{S}_i \cdot \boldsymbol{S}_j \times \boldsymbol{S}_k$ [1,4,13], whereas the spin Hall effect [9] and electrical magnetochiral effects [12] are related to the vector spin chirality of two spins $\boldsymbol{S}_i \times \boldsymbol{S}_j$. These phenomena play an important role in the transport properties of ferromagnetic materials with long-range magnetic structures. The AHE related to scalar spin chirality has been intensively studied in materials hosting magnetic skyrmions [Figs. 1(a) and 1(b)], such as B20 compounds [14–16], pyrochlore magnets [3,17], and Mn_3Sn [18]. On the other hand, the electrical magnetochiral effect has been reported in magnets with helical magnetic order [10,11]. While most of the early works ignored the effect of spin-orbit interaction (SOI) of electronic bands, recent studies pointed out that the SOI gives rise to nontrivial contributions to the AHE by skyrmions [19–21], such as chiral Hall effect (CHE) and monopole contributions. These studies revealed nontrivial effects of SOI in noncentrosymmetric two-band models, such as Rashba and Dresselhaus models.

AHE by magnetic textures also occurs in centrosymmetric materials as skyrmion and magnetic helixes also appear in centrosymmetric materials, such as in frustrated [22,23] and itinerant magnets [24]. These mechanisms not only broaden the list of candidate materials but are also favorable for realizing a large chirality-related AHE. In the case of frustrated magnets, the size of the skyrmion stabilized by these mechanisms is governed by the ratio of competing exchange interactions, typically the nearest- and further-neighbor interactions, and by the Fermi wave number in the case of itinerant magnets. In both cases, the typical size of a skyrmion is smaller than those stabilized by the Dzyaloshinskii-Moriya interaction in noncentrosymmetric materials, in which case the skyrmion radius λ is related to the ratio of ferromagnetic exchange and Dzyaloshinskii-Moriya interaction, $\lambda = 10 - 100$ nm [25]. As the magnitude of AHE by skyrmions is proportional to the density of the skyrmion [25], a smaller skyrmion radius is favorable for realizing a larger AHE. In fact, some centrosymmetric skyrmion materials show a very large topological Hall effect [26]. As with noncentrosymmetric materials, SOI may affect the chirality-related AHE in centrosymmetric materials. However, while several works have studied the effects of SOI on the AHE in coplanar magnets [27,28], the role of inversion symmetry remains unclear.

In this paper, we theoretically study the AHE by magnetic textures in a centrosymmetric magnet with SOI. Considering

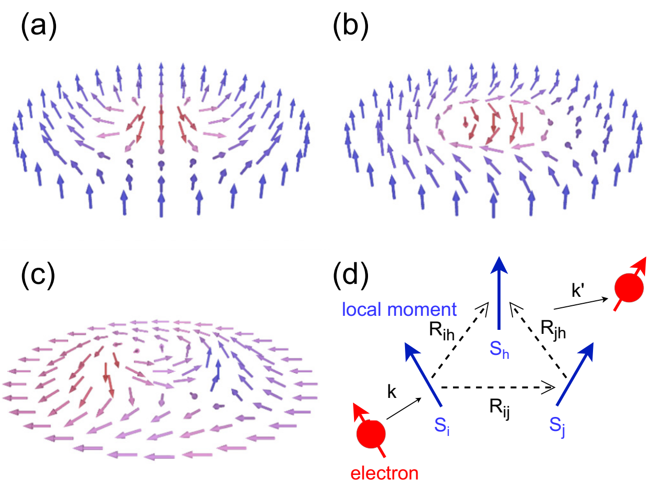

FIG. 1. Schematics of (a) Neel- and (b) Bloch-type magnetic skyrmion and (c) Neel-type bimeron studied in this paper. (d) A schematic of electron scattering by multiple local moments.

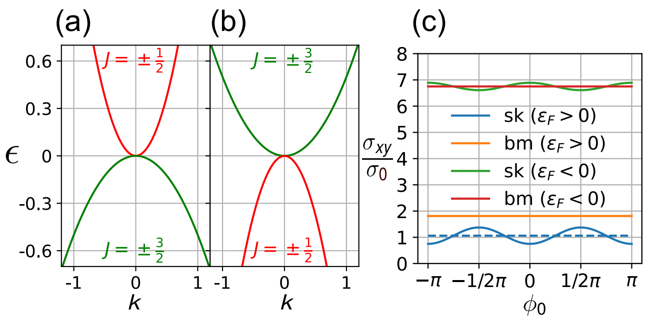

FIG. 2. The band structure of the Luttinger model with $\alpha = 0.5$, (a) $m = 1/2$, and (b) $m = -1/2$. (c) Helicity dependence of chirality-related anomalous Hall conductivity in skyrmion and bimeron crystals with $M_z = \alpha = 0$, $S = n_{\rm sk} = q = 1$. In the figure, sk and bm denote skyrmion and bimeron, respectively.

the two-dimensional Luttinger model [29] as the effective Hamiltonian for itinerant electrons, we study the AHE induced by long-range magnetic textures using a scattering theory method. We show that the AHE related to scalar spin chirality is suppressed by more than one order of magnitude compared to the simple quadratic Hamiltonian without SOI, and the contribution discovered in the Rashba model vanishes. On the other hand, a different contribution related to vector spin chirality appears that gives rise to the difference in the Hall conductivity in Bloch and Neel skyrmion crystals, thereby enabling electrical distinction between the two types of skyrmions [Fig. 2(c)]. The effect of SOI on AHE by bimerons is also discussed.

Model and method.

a. Luttinger Kondo-lattice model. As an example of the centrosymmetric semiconductor with SOI, we consider a two-dimensional variant of the Luttinger model coupled to classical spins. The Hamiltonian reads

$$H = H_0 + H_K, \tag{1}$$

where

$$H_0 = \sum_{\boldsymbol{k},\mu,\nu} c_\mu^\dagger(\boldsymbol{k})\left[\frac{k^2}{2\tilde{M}} + \frac{\frac{5}{4}k^2 - (k_xJ_x + k_yJ_y)^2}{2m}\right]_{\mu\nu} c_\nu(\boldsymbol{k}) \tag{2}$$

is the effective Hamiltonian for itinerant electrons described by the Luttinger Hamiltonian [29] and

$$H_K = J_K \sum_i c_\mu^\dagger(\boldsymbol{R}_i)(\boldsymbol{S}_i\cdot\boldsymbol{J})_{\mu\nu} c_\nu(\boldsymbol{R}_i) \tag{3}$$

is the Kondo coupling between the classical localized spins and itinerant electrons. Here $c_\mu(\boldsymbol{k})$ $[c_\mu^\dagger(\boldsymbol{k})]$ is the annihilation [creation] operator of an electron with momentum $\boldsymbol{k} = (k_x, k_y)$ and spin μ, $k = |\boldsymbol{k}|$, $\boldsymbol{J} = (J_x, J_y, J_z)$ is the vector of $J = 3/2$ spin operators J_a $(a = x, y, z)$, $\boldsymbol{S}_i = (S_i^x, S_i^y, S_i^z)$ is the ith localized moment at position $\boldsymbol{R}_i = (R_i^x, R_i^y)$, and J_K is the strength of exchange coupling between the itinerant electrons and the localized moment. In H_0, the first term is the ordinary quadratic term and the second term is the effect of SOI as seen from the $\boldsymbol{k}\cdot\boldsymbol{J}$ form.

The eigenstates of H_0 consist of two doubly degenerate bands [Fig. 2(a)]. When $|m/\tilde{M}| = |\alpha| < 1$, one of the two doubly degenerate bands is holelike and the other becomes electronlike; the electron and hole bands touch at $\boldsymbol{k} = 0$, forming a zero-gap semiconductor state. Such a state is realized in α-Sn [30] and in pyrochlore iridates [31,32]. On the other hand, when $|\alpha| > 1$, both bands are either electronlike ($m\alpha > 0$) or holelike ($m\alpha < 0$). In this paper, we focus on the $|\alpha| < 1$ case, i.e., the case in which one of the two doubly degenerate bands is electronlike and the other is holelike [Figs. 2(a) and 2(b)].

b. Anomalous Hall effect by skew scattering. To study the AHE arising from coupling to magnetic textures, we compute the anomalous Hall conductivity σ_{xy} focusing on the skew scattering contribution [33]. In the Boltzmann theory, the skew scattering is described by the asymmetry of the scattering rate. The scattering rate $W_{\boldsymbol{k}\mu\to\boldsymbol{k}'\nu}$ is the rate of electrons in the $|\boldsymbol{k}\mu\rangle$ state, the μth eigenstate of H_0 with momentum $\boldsymbol{k}$, being scattered to the state $|\boldsymbol{k}'\nu\rangle$. The skew scattering AHE is related to the difference of $W_{\boldsymbol{k}\mu\to\boldsymbol{k}'\nu}$ and its inverse process $W_{\boldsymbol{k}'\nu\to\boldsymbol{k}\mu}$. To study the asymmetry in the scattering rate, we first define the symmetric $w^+_{\boldsymbol{k}\mu\to\boldsymbol{k}'\nu}$ and antisymmetric $w^-_{\boldsymbol{k}\mu\to\boldsymbol{k}'\nu}$ terms of the scattering rate by

$$w^\pm_{\boldsymbol{k}\mu\to\boldsymbol{k}'\nu} = \tfrac{1}{2}(W_{\boldsymbol{k}\mu\to\boldsymbol{k}'\nu} \pm W_{\boldsymbol{k}'\nu\to\boldsymbol{k}\mu}). \tag{4}$$

In this paper, we focus on the asymmetric scattering $w^-_{\boldsymbol{k}\mu\to\boldsymbol{k}'\nu}$ by the magnetic scattering.

Within the second Born approximation, the antisymmetric term $w^-_{\boldsymbol{k}\mu\to\boldsymbol{k}'\nu}$ reads

$$\begin{aligned} w^-_{\boldsymbol{k}\mu\to\boldsymbol{k}'\nu} =& 4\pi^2 \sum_{\boldsymbol{p},\lambda} \mathrm{Im}[\langle\boldsymbol{k}'\nu\,|\,H_K\,|\,\boldsymbol{k}\mu\rangle\langle\boldsymbol{k}\mu\,|\,H_K\,|\,\boldsymbol{p}\lambda\rangle \\ &\times \langle\boldsymbol{p}\lambda\,|\,H_K\,|\,\boldsymbol{k}'\nu\rangle]\delta(\epsilon_{\boldsymbol{k}\mu} - \epsilon_{\boldsymbol{k}'\nu})\delta(\epsilon_{\boldsymbol{k}\mu} - \epsilon_{\boldsymbol{p}\lambda}). \end{aligned} \tag{5}$$

Here we considered H_0 as the unperturbed Hamiltonian and H_K as the perturbation that causes electron scattering. The Hall conductivity is calculated by combining Eq. (5) with the semiclassical Boltzmann theory, as summarized in Appendix A.

Results.

a. Hall conductivity for the electron-doped case. We first consider the electron-doped case ($\epsilon_F \geqslant 0$) assuming a positive electron mass $m > 0$, where ϵ_F is the Fermi energy. The Hall conductivity σ_{xy} reads

$$\begin{aligned} \sigma_{xy} =& -\frac{\sigma_0}{2^{10}(1+\alpha)} \\ &\times [9f_1(\{\boldsymbol{S}_h\}) + 58f_2(\{\boldsymbol{S}_h\}) + 30f_3(\{\boldsymbol{S}_h\})]. \end{aligned} \tag{6}$$

Here,

$$\begin{aligned} f_1(\{\boldsymbol{S}_h\}) =& \frac{1}{L^2}\sum_{h,i,j} S_h^z\big[8S_i^zS_j^z\boldsymbol{R}_{ih}\cdot\boldsymbol{R}_{jh} \\ &+ (\boldsymbol{S}_i\cdot\boldsymbol{S}_j)\big(17\boldsymbol{R}_{ih}\cdot\boldsymbol{R}_{jh} - 5R_{ih}^2 - 5R_{jh}^2\big)\big], \\ f_2(\{\boldsymbol{S}_h\}) =& \frac{1}{L^2}\sum_{h,i,j}(\boldsymbol{S}_h\cdot\boldsymbol{S}_i\times\boldsymbol{S}_j)(\boldsymbol{R}_{ih}\times\boldsymbol{R}_{jh}\cdot\hat{z}), \end{aligned}$$

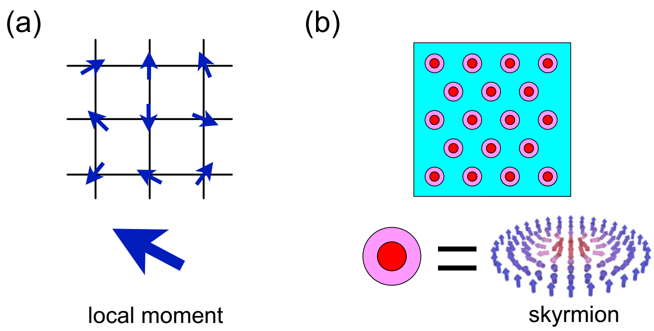

FIG. 3. A schematic of (a) local spins on the square lattice and (b) an example of skyrmion crystal.

$$f_3(\{\boldsymbol{S}_h\}) = \frac{1}{L^2}\sum_{h,i,j}(\boldsymbol{S}_h\cdot\boldsymbol{R}_{ij})[\boldsymbol{S}_i\times\boldsymbol{S}_j\cdot(\boldsymbol{R}_{ih}+\boldsymbol{R}_{jh})\times\hat{z}] + (\boldsymbol{S}_h\cdot\boldsymbol{R}_{ij}\times\hat{z})[\boldsymbol{S}_i\times\boldsymbol{S}_j\cdot(\boldsymbol{R}_{ih}+\boldsymbol{R}_{jh})],$$

and $\sigma_0 = \frac{\tau^2 e^2|m|^3 J_K^3\epsilon_F^2}{2\pi}$, where $\hat{z}$ is the unit vector along the z axis, $\boldsymbol{R}_{ij} = \boldsymbol{R}_i - \boldsymbol{R}_j$, L^2 is the area of the system, τ is the relaxation time for symmetric scattering, and e is electric charge. Among three terms, $f_1(\{\boldsymbol{S}_h\})$ corresponds to a generalization of the skew scattering AHE by magnetic scattering [34] and $f_2(\{\boldsymbol{S}_h\})$ is the skew scattering AHE related to the scalar spin chirality $\boldsymbol{S}_h\cdot\boldsymbol{S}_i\times\boldsymbol{S}_j$ [13]. The third term $f_3(\{\boldsymbol{S}_h\})$ is the AHE related to the vector spin chirality $\boldsymbol{S}_i\times\boldsymbol{S}_j$, which is the term describing the interplay of magnetic texture and SOI.

To see how the SOI affects the AHE, we compare Eq. (6) to the anomalous Hall conductivity of a model without SOI. To this end, we consider a quadratic Hamiltonian

$$\tilde{H}_0 = \sum_{\boldsymbol{k}} c_\mu(\boldsymbol{k})^\dagger \frac{k^2}{2\tilde{m}} c_\mu(\boldsymbol{k}). \tag{7}$$

The dispersion of $\tilde{H}_0$ is exactly the same as that of H_0 when $\tilde{m} = m/(1+\alpha)$. Therefore, comparing the anomalous Hall conductivity of two models helps us clarify the effect of SOI. The scattering rate and Hall conductivity for $\tilde{H}_0$ reads

$$\tilde{\sigma}_{xy} = -\frac{\sigma_0}{1+\alpha} f_2(\{\boldsymbol{S}_h\}), \tag{8}$$

when $\tilde{m} = m/(1+\alpha)$. The result resembles $f_2(\{\boldsymbol{S}_h\})$ term in σ_{xy}. However, the magnitude in Eq. (6) is reduced by $29/512 \sim 1/18$ compared to the case without SOI. The result indicates that the AHE related to scalar spin chirality in the Luttinger model is suppressed by more than one order of magnitude compared to that without SOI.

b. Continuum limit for the electron-doped case. We next turn to a spin texture slowly varying in space, such as in ferromagnets with magnetic skyrmions. To be concrete, we consider a square lattice magnet [Fig. 3(a)]. When the spins vary slowly in space, $\boldsymbol{S}_i$ near $\boldsymbol{S}_h$ can be approximated as $\boldsymbol{S}_i \sim \boldsymbol{S}_h + (\boldsymbol{R}_{ih}\cdot\nabla)\boldsymbol{S}_h + \frac{1}{2}(\boldsymbol{R}_{ih}\cdot\nabla)^2\boldsymbol{S}_h$. To evaluate the Hall conductivity, we assume that the contribution from the multiple-spin scattering due to nearest-neighbor sites is dominant. That is, we limit i and j to the nearest-neighbor sites of h. By using the gradient expansion, replacing $\sum_h$ by $\int \frac{dxdy}{a^2}$ and $\boldsymbol{S}_h$ by $\boldsymbol{S} = (S^x(r), S^y(r), S^z(r))$, we obtain

$$\sigma_{xy}^{(h)} = \frac{\sigma_0}{(1+\alpha)L^2}\int dxdy\, \frac{45}{32}S^zS^2 - \frac{153}{256}a^2S^z(|\partial_x\boldsymbol{S}|^2+|\partial_y\boldsymbol{S}|^2) + \frac{45}{64}a^2S^z\boldsymbol{S}\cdot\Delta\boldsymbol{S} - \frac{9}{32}a^2S^z(|\partial_xS^z|^2+|\partial_yS^z|^2)$$
$$-\frac{29}{64}\frac{\sigma_0 a^2}{(1+\alpha)L^2}\int dxdy\, \boldsymbol{S}\cdot\partial_x\boldsymbol{S}\times\partial_y\boldsymbol{S} + \frac{15}{128}\frac{\sigma_0 a^2}{(1+\alpha)L^2}\int dxdy\, \left(S^x\left[\left(\partial_x^2-\partial_y^2\right)\boldsymbol{S}\times\boldsymbol{S}\right]_y + S^y\left[\left(\partial_x^2-\partial_y^2\right)\boldsymbol{S}\times\boldsymbol{S}\right]_x\right), \tag{9}$$

where a is the lattice constant that defines the distance between nearest-neighbor spins and $S = |\boldsymbol{S}|$.

Compared to noncentrosymmetric models [19,21], no term with one spatial derivative of spin exists in Eq. (9), namely, the contributions similar to CHE [19] and monopole [21] contributions are absent. The absence of linear-in-gradient terms is understandable from the symmetry of H. Phenomenologically, Eq. (9) indicates that the Hall current follows $J_y = \sigma' f(\{\boldsymbol{S}(\boldsymbol{r})\})E_x$, where $f(\{\boldsymbol{S}(\boldsymbol{r})\})$ is a functional of spins. For concreteness, let us consider $f(\{\boldsymbol{S}(\boldsymbol{r})\}) = (S^x)^2\partial_x S^x$. In this case, the inversion operation transforms $J_y = \sigma' f(\{\boldsymbol{S}(\boldsymbol{r})\})E_x \;\to\; J_y = -\sigma' f(\{\boldsymbol{S}(\boldsymbol{r})\})E_x$. Hence, $\sigma' = 0$. The same argument holds for arbitrary $f(\{\boldsymbol{S}(\boldsymbol{r})\})$ with one spatial derivative. Hence, the AHE related to terms with one spatial derivative, e.g., CHE and monopole contributions, is prohibited in a centrosymmetric system. In contrast, two-derivative terms, such as $S^x[(-\partial_x^2+\partial_y^2)\boldsymbol{S}\times\boldsymbol{S}]_y + S^y[(-\partial_x^2+\partial_y^2)\boldsymbol{S}\times\boldsymbol{S}]_x$ and $\boldsymbol{S}\cdot\partial_x\boldsymbol{S}\times\partial_y\boldsymbol{S}$, are allowed by symmetry. Therefore, the absence of the CHE and monopole contribution reflects the inversion symmetry of the model.

c. Magnetic skyrmions and bimerons. To gain insight into how the unique term affects AHE in skyrmion materials, we apply Eq. (9) to a skyrmion crystal state. Here we consider a crystal of a magnetic skyrmion whose spin configuration is

$$\boldsymbol{S} = S\left(\frac{2\lambda r\cos(q\phi-\phi_0)}{r^2+\lambda^2}, \frac{2\lambda r\sin(q\phi-\phi_0)}{r^2+\lambda^2}, \frac{r^2-\lambda^2}{r^2+\lambda^2}\right), \tag{10}$$

where r is the distance from the skyrmion center, λ is the skyrmion radius, ϕ is the azimuth angle [35], ϕ_0 is the helicity of the skyrmion, and $q = \pm 1$ is the skyrmion charge [25]. When $\phi_0 = 0, \pi$, the skyrmion is Neél type, and when $\phi_0 = \pm\pi/2$, it is Bloch type [see Figs. 1(a) and 1(b)]. A periodic alignment, or a crystal, of skyrmions [see Fig. 3(b)] is known to be stable in many magnetic materials [36,37], which has been intensively explored over the last couple of decades [38–40].

By using Eq. (9), the anomalous Hall conductivity of the skyrmion crystal reads

$$\sigma_{xy} = \frac{\sigma_0 S^3}{32(1+\alpha)}[45M_z + n_{\rm sk}[34q - 10\cos(2\phi_0)]], \quad (11)$$

where M_z is the out-of-plane magnetization per area and $n_{\rm sk}$ is the skyrmion density. The term proportional to $n_{\rm sk}q$ contains the contribution from $S^z(|\partial_x S^z|^2 + |\partial_y S^z|^2)$ and scalar spin chirality $\boldsymbol{S}\cdot\partial_x\boldsymbol{S}\times\partial_y\boldsymbol{S}$, whereas the third term proportional to $n_{\rm sk}\cos(2\phi_0)$ is the contribution from SOI. The $\cos(2\phi_0)$ dependence of the third term indicates that the Hall conductivity depends on the helicity; the term gives a negative contribution to AHE in Neel-type skyrmion and a positive contribution to Bloch type [Fig. 2(c)]. Hence, the f_3 term, which arises from the interplay of SOI and magnetic texture, enables the detection of the skyrmion helicity.

As another example of nontrivial magnetic texture, we consider a bimeron crystal whose spin orientation reads [Fig. 1(c)]

$$\boldsymbol{S} = S\left(\frac{r^2-\lambda^2}{r^2+\lambda^2}, \frac{2\lambda r\sin(q\phi-\phi_0)}{r^2+\lambda^2}, -\frac{2\lambda r\cos(q\phi-\phi_0)}{r^2+\lambda^2}\right). \quad (12)$$

Intuitively, magnetic bimeron is a skyrmion whose spins are rotated by $\pi/2$ about the x or y axis [41]. The anomalous Hall conductivity for the bimeron crystal reads

$$\sigma_{xy} = \frac{29}{16}\frac{\sigma_0}{1+\alpha}n_{\rm sk}qS^3. \quad (13)$$

Unlike the magnetic skyrmion case, only the $f_2(\{\boldsymbol{S}_h\})$ term contributes to the AHE in the bimeron crystal.

d. Hole-doped case. We next consider the hole-doped case ($\epsilon_F \leqslant 0$), assuming $m > 0$. The Hall conductivity reads

$$\sigma_{xy} = \frac{27\sigma_0}{2^9(1-\alpha)}\left[f_1'(\{\boldsymbol{S}_h\}) - 4f_2(\{\boldsymbol{S}_h\}) + \frac{1}{4}f_3(\{\boldsymbol{S}_h\})\right], \quad (14)$$

where

$$f_1'(\{\boldsymbol{S}_h\}) = \frac{1}{L^2}\sum_{h,i,j} S_h^z[(\boldsymbol{S}_i\cdot\boldsymbol{S}_j)(R_{ih}^2 + R_{jh}^2 - 6\boldsymbol{R}_{ih}\cdot\boldsymbol{R}_{jh})].$$

In the continuum limit, the Hall conductivity reads

$$\sigma_{xy} = \frac{\sigma_0}{(1-\alpha)L^2}\int dxdy\, \frac{27}{16}S^zS^2 - \frac{81}{64}a^2S^z(|\partial_x\boldsymbol{S}|^2 + |\partial_y\boldsymbol{S}|^2) + \frac{27}{32}a^2S^z\boldsymbol{S}\cdot\Delta\boldsymbol{S} - \frac{27\sigma_0}{16(1-\alpha)L^2}\int dxdy\, \boldsymbol{S}\cdot\partial_x\boldsymbol{S}\times\partial_y\boldsymbol{S}$$
$$- \frac{27\sigma_0}{512(1-\alpha)L^2}\int dxdy\,\left(S^x\left[(\partial_x^2-\partial_y^2)\boldsymbol{S}\times\boldsymbol{S}\right]_y + S^y\left[(\partial_x^2-\partial_y^2)\boldsymbol{S}\times\boldsymbol{S}\right]_x\right). \quad (15)$$

Compared to the electron-doped case, the f_2 term becomes relatively large compared to f_3, i.e., the topological Hall effect becomes larger compared to the effect of SOI in the hole-doped case.

By using this equation, the anomalous Hall conductivity of the skyrmion crystal reads

$$\sigma_{xy} = \frac{27\sigma_0S^3}{32(1-\alpha)}\left[2M_z + n_{\rm sk}\left(8q + \frac{\cos(2\phi_0)}{6}\right)\right], \quad (16)$$

and the anomalous Hall conductivity of the bimeron crystal reads

$$\sigma_{xy} = \frac{27}{4}\frac{\sigma_0}{1-\alpha}n_{\rm sk}qS^3. \quad (17)$$

As expected from Eq. (14), the helicity dependence of σ_{xy} for the skyrmion crystal becomes smaller compared to the electron-doped case and with the opposite sign, as shown in Fig. 2(c).

e. $m < 0$ case. When $m < 0$, the same calculation gives Eqs. (14) and (15) for $\varepsilon_F > 0$, and Eqs. (6) and (9) for $\varepsilon_F < 0$, i.e., the result for electron- and hole-doped cases inverts [Fig. 2(a)]. It reflects the fact that the orbitals for electron and hole bands invert by changing the sign of m. Hence, the behavior of AHE in the $m < 0$ case is qualitatively the same as those discussed above.

Note that this behavior is distinct from the Rashba model [19,21], where changing the sign of SOI changes the sign of AHE. For the case of Rashba model, inverting the sign of SOI only changes the spin texture in the momentum space; the electron dispersion remains exactly the same. On the other hand, the four bands in the Luttinger model are usually the bands that split off from six or more degenerated bands in the absence of SOI [42]. In such a case, changing the sign of SOI inverts the orbitals, leading to a behavior more complicated than the Rashba model. Hence, the AHE in Luttinger model shows distinct behavior compared to the Rashba model.

Summary. In this paper, we studied the skew scattering and AHE in a two-dimensional Luttinger model coupled to localized moments by the Kondo coupling. Using a scattering theory method, we derived a general formula for the anomalous Hall conductivity, which consists of three terms: the AHE proportional to the magnetization, topological Hall effect (THE), and vector spin chirality term. The result shows that THE in the Luttinger model is suppressed by more than one order of magnitude compared to the quadratic band electron. On the other hand, the vector spin chirality term is a contribution arising from the interplay of SOI and nontrivial magnetic texture. This term, however, is distinct from those known in noncentrosymmetric models such as CHE related to vector spin chirality [19] and monopole contribution [21]. This is evident from the fact that only the second-order derivative of spins appears in the continuum limit, in contrast to the vector spin chirality $\boldsymbol{S}\times\nabla\boldsymbol{S}$ and magnetic monopole $\nabla\cdot\boldsymbol{S}$ terms in noncentrosymmetric magnets. These terms give rise to the helicity dependence of anomalous Hall conductivity in the case of skyrmion crystals, hence enabling the electrical distinction of Bloch and Neel skyrmions. In the case of bimeron crystals, however, only the THE term contributes to the AHE. Hence, there is no helicity dependence. The results demonstrate the rich effect of SOI and crystal symmetry on the AHE by nontrivial spin texture.

The helicity dependence of anomalous Hall conductivity suggests that the AHE is a potential probe for detecting skyrmion helicity. Compared to those using optical techniques [43], the detection by transport phenomena has advantages for applications, such as the simplicity of device structure. Our result demonstrates that the anomalous Hall conductivity changes depending on the type of skyrmion, Neel type or Bloch type. For the application, if $m > 0$, the electron-doped case might be a better candidate as the helicity-dependent contribution is relatively large compared to other contributions.

Lastly, we briefly discuss the effect of anisotropy. In general, a uniaxial anisotropy term proportional to $(J^z)^2$ exists in the two-dimensional Luttinger model. We, however, expect that the anisotropy does not change the main conclusions of this paper, such as the absence of linear-in-gradient terms, as they are the consequences of inversion symmetry. We also note that, if the anisotropy is sufficiently smaller than the chemical potential μ, the wave function of the electrons near the Fermi level remains almost the same as that without anisotropy. Hence, the anisotropy term does not change the scattering rate and the transport coefficients. Therefore, we expect our result to be quantitatively valid when the anisotropy is small, and qualitatively the same even with a large anisotropy.

Acknowledgments. We are grateful for the fruitful discussions with J. Fujii, N. Kanazawa, and J. Mochida. This work was supported by JSPS KAKENHI (Grants No. JP19K14649 and No. JP23K03275).

Appendix A: Boltzmann theory. The calculation of Hall conductivity follows a paper by one of the authors [13]. In the Boltzmann theory, the electron distribution was evaluated by the Boltzmann equation. In the presence of the uniform static electric field in x direction, the Boltzmann equation reads

$$\frac{(1+\alpha)ek\cos\theta_k E_x}{m} f_0'(\epsilon_{\boldsymbol{k}}) = \frac{g_{\boldsymbol{k}\mu}}{\tau} + \frac{L^2}{4\pi^2}\sum_\nu \int dk' d\theta_{k'}\; w^-_{\boldsymbol{k}\mu\to\boldsymbol{k}'\nu} g_{\boldsymbol{k}'\nu}, \tag{A1}$$

where $\theta_k = \tan^{-1}(k_y/k_x)$, E_x is the external electric field, and $f_0(\epsilon_{\boldsymbol{k}})$ and $f_0'(\epsilon_{\boldsymbol{k}})$ are the Fermi-Dirac distribution function and its energy derivative, respectively. Here, we assumed that the electron occupation $f_{\boldsymbol{k}\mu} = f_0(\epsilon_{\boldsymbol{k}}) + g_{\boldsymbol{k}\mu}$ is close to that of the Fermi-Dirac distribution and expanded to the equation up to leading order in E_x, assuming $g_{\boldsymbol{k}\mu} = O(E_x)$. In addition, in Eq. (A1), we used the relaxation time approximation for the symmetric part of the scattering rate $w^+_{\boldsymbol{k}\mu\to\boldsymbol{k}'\nu}$, i.e., $w^+_{\boldsymbol{k}\mu\to\boldsymbol{k}'\nu}$ is replaced by $-\frac{g_{\boldsymbol{k}\mu}}{\tau}$, where τ is the relaxation time.

Here, we assume the form

$$w^-_{\boldsymbol{k}\mu\to\boldsymbol{k}'\nu} = \sum_n c_n \sin n\phi, \tag{A2}$$

where $\phi = \theta_{k'} - \theta_k$ is the angle between $\boldsymbol{k}$ and $\boldsymbol{k}'$. This is a generalization of the antisymmetric scattering term. Solving Eq. (A1) up to leading order in $w^-_{\boldsymbol{k}\mu\to\boldsymbol{k}'\nu}$, $g_{\boldsymbol{k}\mu}$ reads

$$g_{\boldsymbol{k}\mu} = \frac{(1+\alpha)\tau ek\cos\theta_k E_x}{m} f_0'(\epsilon_{\boldsymbol{k}}) + \frac{(1+\alpha)\tau e L^2 E_x}{4\pi^2 m} \times \sum_{\nu,n} c_n \int k' f_0'(\epsilon_{\boldsymbol{k}'})\, dk' \int \sin n\phi \cos\theta_{k'}\, d\theta_{k'}. \tag{A3}$$

Since $\int \sin n\phi \cos\theta_{k'}\, d\theta_{k'} = -\frac{\sin\theta_k}{2}\delta_{n,1}$, only the c_1 term in Eq. (A2) remains, i.e., among the asymmetric scattering terms, only those proportional to $\sin\phi$ contribute to Hall conductivity.

Appendix B: Anomalous Hall conductivity. Using Eq. (5) in the main text, the antisymmetric scattering term $w^-_{\boldsymbol{k}\mu\to\boldsymbol{k}'\nu}$ for the hole-doped case reads

$$w^-_{\boldsymbol{k}\mu\to\boldsymbol{k}'\nu} = \frac{27\pi|m|J_K^3}{2^9(1-\alpha)L^4} V_{\mu\nu}\delta(\epsilon_{\boldsymbol{k}\mu} - \epsilon_{\boldsymbol{k}'\nu}), \tag{B1}$$

where

$$\boldsymbol{V} = V_0\sigma_0 + V_x\sigma_x + V_y\sigma_y + V_z\sigma_z, \tag{B2}$$

and

$$\begin{aligned} V_0 = {}& S_h^z(\boldsymbol{S}_i\cdot\boldsymbol{S}_j)(\sin\phi + 2\sin 2\phi + \sin 3\phi) \\ &+ k^2 S_h^z(\boldsymbol{S}_i\cdot\boldsymbol{S}_j)\tfrac{1}{4}\big[R_{ij}^2(\sin\phi - 4\sin 2\phi - 3\sin 3\phi) + \boldsymbol{R}_{ih}\cdot\boldsymbol{R}_{jh}(-4\sin\phi + 2\sin 2\phi + 4\sin 3\phi + \sin 4\phi)\big] \\ &+ k^2(\boldsymbol{R}_{ih}\times\boldsymbol{R}_{jh}\cdot\hat{z})[\boldsymbol{S}_h\cdot\boldsymbol{S}_i\times\boldsymbol{S}_j(2\sin\phi + \sin 2\phi) + S_h^z(\boldsymbol{S}_i\times\boldsymbol{S}_j\cdot\hat{z})\tfrac{1}{4}(-4\sin\phi + 2\sin 2\phi + 4\sin 3\phi + \sin 4\phi)] \\ &+ k^2[(\boldsymbol{S}_h\cdot\boldsymbol{R}_{ij})\{\boldsymbol{S}_i\times\boldsymbol{S}_j\cdot(\boldsymbol{R}_{ih}+\boldsymbol{R}_{jh})\times\hat{z}\} + (\boldsymbol{S}_h\cdot\boldsymbol{R}_{ij}\times\hat{z})\{\boldsymbol{S}_i\times\boldsymbol{S}_j\cdot(\boldsymbol{R}_{ih}+\boldsymbol{R}_{jh})\}]\tfrac{1}{8}(3\sin\phi - \sin 3\phi), \end{aligned} \tag{B3}$$

$$\begin{aligned} V_x = {}& S_h^z(\boldsymbol{S}_i\cdot\boldsymbol{S}_j)(-\sin\phi + 2\sin 2\phi + \sin 3\phi) \\ &+ k^2 S_h^z(\boldsymbol{S}_i\cdot\boldsymbol{S}_j)\tfrac{1}{4}\big[R_{ij}^2(-5\sin\phi + 4\sin 2\phi - \sin 3\phi) + \boldsymbol{R}_{ih}\cdot\boldsymbol{R}_{jh}(20\sin\phi - 20\sin 2\phi + 8\sin 3\phi - \sin 4\phi)\big] \\ &+ k^2(\boldsymbol{R}_{ih}\times\boldsymbol{R}_{jh}\cdot\hat{z})[\boldsymbol{S}_h\cdot\boldsymbol{S}_i\times\boldsymbol{S}_j(2\sin\phi - \sin 2\phi) + S_h^z(\boldsymbol{S}_i\times\boldsymbol{S}_j\cdot\hat{z})\tfrac{1}{4}(4\sin\phi + 2\sin 2\phi - 4\sin 3\phi + \sin 4\phi)] \\ &+ k^2[(\boldsymbol{S}_h\cdot\boldsymbol{R}_{ij})\{\boldsymbol{S}_i\times\boldsymbol{S}_j\cdot(\boldsymbol{R}_{ih}+\boldsymbol{R}_{jh})\times\hat{z}\} + (\boldsymbol{S}_h\cdot\boldsymbol{R}_{ij}\times\hat{z})\{\boldsymbol{S}_i\times\boldsymbol{S}_j\cdot(\boldsymbol{R}_{ih}+\boldsymbol{R}_{jh})\}]\tfrac{1}{8}(-5\sin\phi + 4\sin 2\phi - \sin 3\phi), \end{aligned} \tag{B4}$$

$$V_y = -ik\boldsymbol{S}_h \times (\boldsymbol{S}_i \times \boldsymbol{S}_j) \cdot \boldsymbol{R}_{ij}(-3\cos\phi + 4\cos 2\phi - \cos 3\phi), \tag{B5}$$

$$V_z = -k(\boldsymbol{S}_h \cdot \boldsymbol{R}_{ij})(\boldsymbol{S}_i \times \boldsymbol{S}_j \cdot \hat{z})(5\sin\phi + 4\sin 2\phi + \sin 3\phi) + kS_h^z(\boldsymbol{S}_i \times \boldsymbol{S}_j \cdot \boldsymbol{R}_{ij})(\sin\phi + 2\sin 2\phi + \sin 3\phi). \tag{B6}$$

Among the asymmetric scattering terms, only those proportional to $\sin\phi$ contribute to Hall conductivity, as discussed in Appendix A. Therefore, we focus on the terms proportional to $\sin\phi$,

$$\tilde{w}^-_{\boldsymbol{k}\mu\to\boldsymbol{k}'\nu} = \frac{27\pi|m|J_K^3}{2^9(1-\alpha)L^4}\tilde{V}_{\mu\nu}\sin\phi\,\delta(\epsilon_{\boldsymbol{k}\mu} - \epsilon_{\boldsymbol{k}'\nu}), \tag{B7}$$

where

$$\tilde{\boldsymbol{V}} = \tilde{V}_0\sigma_0 + \tilde{V}_x\sigma_x + \tilde{V}_y\sigma_y + \tilde{V}_z\sigma_z, \tag{B8}$$

and

$$\begin{aligned}\tilde{V}_0 =& S_h^z(\boldsymbol{S}_i \cdot \boldsymbol{S}_j) + k^2S_h^z(\boldsymbol{S}_i \cdot \boldsymbol{S}_j)\tfrac{1}{4}\big[R_{ij}^2 - 4\boldsymbol{R}_{ih}\cdot\boldsymbol{R}_{jh}\big] + k^2(\boldsymbol{R}_{ih}\times\boldsymbol{R}_{jh}\cdot\hat{z})\big[2\boldsymbol{S}_h\cdot\boldsymbol{S}_i\times\boldsymbol{S}_j - S_h^z(\boldsymbol{S}_i\times\boldsymbol{S}_j\cdot\hat{z})\big]\\ &+ \tfrac{3}{8}k^2[(\boldsymbol{S}_h\cdot\boldsymbol{R}_{ij})\{\boldsymbol{S}_i\times\boldsymbol{S}_j\cdot(\boldsymbol{R}_{ih}+\boldsymbol{R}_{jh})\times\hat{z}\} + (\boldsymbol{S}_h\cdot\boldsymbol{R}_{ij}\times\hat{z})\{\boldsymbol{S}_i\times\boldsymbol{S}_j\cdot(\boldsymbol{R}_{ih}+\boldsymbol{R}_{jh})\}],\end{aligned} \tag{B9}$$

$$\begin{aligned}\tilde{V}_x =& -S_h^z(\boldsymbol{S}_i \cdot \boldsymbol{S}_j) + k^2S_h^z(\boldsymbol{S}_i \cdot \boldsymbol{S}_j)\tfrac{5}{4}[-R_{ij}^2 + 4\boldsymbol{R}_{ih}\cdot\boldsymbol{R}_{jh}] + k^2(\boldsymbol{R}_{ih}\times\boldsymbol{R}_{jh}\cdot\hat{z})\big[2\boldsymbol{S}_h\cdot\boldsymbol{S}_i\times\boldsymbol{S}_j + S_h^z(\boldsymbol{S}_i\times\boldsymbol{S}_j\cdot\hat{z})\big]\\ &- \tfrac{5}{8}k^2[(\boldsymbol{S}_h\cdot\boldsymbol{R}_{ij})\{\boldsymbol{S}_i\times\boldsymbol{S}_j\cdot(\boldsymbol{R}_{ih}+\boldsymbol{R}_{jh})\times\hat{z}\} + (\boldsymbol{S}_h\cdot\boldsymbol{R}_{ij}\times\hat{z})\{\boldsymbol{S}_i\times\boldsymbol{S}_j\cdot(\boldsymbol{R}_{ih}+\boldsymbol{R}_{jh})\}],\end{aligned} \tag{B10}$$

$$\tilde{V}_y = 0, \tag{B11}$$

$$\tilde{V}_z = -5k(\boldsymbol{S}_h\cdot\boldsymbol{R}_{ij})(\boldsymbol{S}_i\times\boldsymbol{S}_j\cdot\hat{z}) + kS_h^z(\boldsymbol{S}_i\times\boldsymbol{S}_j\cdot\boldsymbol{R}_{ij}). \tag{B12}$$

By using these equations and the semiclassical Boltzmann theory, the Hall conductivity σ_{xy} for the hole-doped case reads

$$\sigma_{xy} = -\frac{27\tau^2e^2|m|mJ_K^3\epsilon_F}{2^{11}\pi(1-\alpha)L^2}(\tilde{V}_0 + \tilde{V}_x)|_{k=\sqrt{-2m\epsilon_F}}, \tag{B13}$$

where

$$\tilde{V}_0 + \tilde{V}_x = k^2\big[f_1'(\{\boldsymbol{S}_h\}) - 4f_2(\{\boldsymbol{S}_h\}) + \tfrac{1}{4}f_3(\{\boldsymbol{S}_h\})\big]. \tag{B14}$$

The Hall conductivity for the electron-doped case was calculated in the same way as in the hole-doped case. For the electron-doped case, the Hall conductivity reads

$$\sigma_{xy} = \frac{\tau^2e^2|m|mJ_K^3\epsilon_F}{2^{11}\pi(1+\alpha)L^2}(\tilde{V}_0 + \tilde{V}_x)|_{k=\sqrt{2m\epsilon_F}}, \tag{B15}$$

where

$$\tilde{V}_0 + \tilde{V}_x = -k^2[9f_1(\{\boldsymbol{S}_h\}) + 58f_2(\{\boldsymbol{S}_h\}) + 30f_3(\{\boldsymbol{S}_h\})]. \tag{B16}$$

[1] J. Ye, Y. B. Kim, A. J. Millis, B. I. Shraiman, P. Majumdar, and Z. Tešanović, Berry phase theory of the anomalous Hall effect: Application to colossal magnetoresistance manganites, Phys. Rev. Lett. **83**, 3737 (1999).

[2] K. Ohgushi, S. Murakami, and N. Nagaosa, Spin anisotropy and quantum Hall effect in the *kagomé* lattice: Chiral spin state based on a ferromagnet, Phys. Rev. B **62**, R6065(R) (2000).

[3] Y. Taguchi, Y. Oohara, H. Yoshizawa, N. Nagaosa, and Y. Tokura, Spin chirality, Berry phase, and anomalous Hall effect in a frustrated ferromagnet, Science **291**, 2573 (2001).

[4] G. Tatara and H. Kawamura, Chirality-driven anomalous Hall effect in weak coupling regime, J. Phys. Soc. Jpn. **71**, 2613 (2002).

[5] N. Nagaosa, J. Sinova, S. Onoda, A. H. MacDonald, and N. P. Ong, Anomalous Hall effect, Rev. Mod. Phys. **82**, 1539 (2010).

[6] E. Liu, Y. Sun, N. Kumar, L. Muechler, A. Sun, L. Jiao, S.-Y. Yang, D. Liu, A. Liang, Q. Xu, J. Kroder, V. Süß, H. Borrmann, C. Shekhar, Z. Wang, C. Xi, W. Wang, W. Schnelle, S. Wirth, Y. Chen, S. T. B. Goennenwein, and C. Felser, Giant anomalous Hall effect in a ferromagnetic kagome-lattice semimetal, Nat. Phys. **14**, 1125 (2018).

[7] Q. Wang, Y. Xu, R. Lou, Z. Liu, M. Li, Y. Huang, D. Shen, H. Weng, S. Wang, and H. Lei, Large intrinsic anomalous Hall effect in half-metallic ferromagnet $Co_3Sn_2S_2$ with magnetic Weyl fermions, Nat. Commun. **9**, 3681 (2018).

[8] H. Ishizuka and Y. Motome, Spontaneous spatial inversion symmetry breaking and spin Hall effect in a spin-ice double-exchange model, Phys. Rev. B **88**, 100402(R) (2013).

[9] H. Ishizuka and N. Nagaosa, Large anomalous Hall effect and spin Hall effect by spin-cluster scattering in the strong-coupling limit, Phys. Rev. B **103**, 235148 (2021).

[10] T. Yokouchi, N. Kanazawa, A. Kikkawa, D. Morikawa, K. Shibata, T. Arima, Y. Taguchi, F. Kagawa, and Y. Tokura, Electrical magnetochiral effect induced by chiral spin fluctuations, Nat. Commun. **8**, 866 (2017).

[11] R. Aoki, Y. Kousaka, and Y. Togawa, Anomalous nonreciprocal electrical transport on chiral magnetic order, Phys. Rev. Lett. **122**, 057206 (2019).

[12] H. Ishizuka and N. Nagaosa, Anomalous electrical magnetochiral effect by chiral spin-cluster scattering, Nat. Commun. **11**, 2986 (2020).

[13] H. Ishizuka and N. Nagaosa, Spin chirality induced skew scattering and anomalous Hall effect in chiral magnets, Sci. Adv. **4**, eaap9962 (2018).

[14] A. Neubauer, C. Pfleiderer, B. Binz, A. Rosch, R. Ritz, P. G. Niklowitz, and P. Böni, Topological Hall effect in the *A* phase of MnSi, Phys. Rev. Lett. **102**, 186602 (2009).

[15] N. Kanazawa, Y. Onose, T. Arima, D. Okuyama, K. Ohoyama, S. Wakimoto, K. Kakurai, S. Ishiwata, and Y. Tokura, Large topological Hall effect in a short-period helimagnet MnGe, Phys. Rev. Lett. **106**, 156603 (2011).

[16] T. Yokouchi, N. Kanazawa, A. Tsukazaki, Y. Kozuka, M. Kawasaki, M. Ichikawa, F. Kagawa, and Y. Tokura, Stability of two-dimensional skyrmions in thin films of $Mn_{1-x}Fe_xSi$ investigated by the topological Hall effect, Phys. Rev. B **89**, 064416 (2014).

[17] Y. Machida, S. Nakatsuji, Y. Maeno, T. Tayama, T. Sakakibara, and S. Onoda, Unconventional anomalous Hall effect enhanced by a noncoplanar spin texture in the frustrated Kondo lattice $Pr_2Ir_2O_7$, Phys. Rev. Lett. **98**, 057203 (2007).

[18] S. Nakatsuji, N. Kiyohara, and T. Higo, Large anomalous Hall effect in a non-collinear antiferromagnet at room temperature, Nature (London) **527**, 212 (2015).

[19] F. R. Lux, F. Freimuth, S. Blügel, and Y. Mokrousov, Chiral Hall effect in noncollinear magnets from a cyclic cohomology approach, Phys. Rev. Lett. **124**, 096602 (2020).

[20] T. Yamaguchi and A. Yamakage, Theory of magnetic-texture-induced anomalous Hall effect on the surface of topological insulators, J. Phys. Soc. Jpn. **90**, 063703 (2021).

[21] J. Mochida and H. Ishizuka, Skew scattering by magnetic monopoles and anomalous Hall effect in spin-orbit coupled systems, arXiv:2211.10180.

[22] T. Okubo, S. Chung, and H. Kawamura, Multiple-q states and the skyrmion lattice of the triangular-lattice Heisenberg antiferromagnet under magnetic fields, Phys. Rev. Lett. **108**, 017206 (2012).

[23] A. O. Leonov and M. Mostovoy, Multiply periodic states and isolated skyrmions in an anisotropic frustrated magnet, Nat. Commun. **6**, 8275 (2015).

[24] R. Ozawa, S. Hayami, and Y. Motome, Zero-field skyrmions with a high topological number in itinerant magnets, Phys. Rev. Lett. **118**, 147205 (2017).

[25] N. Nagaosa and Y. Tokura, Topological properties and dynamics of magnetic skyrmions, Nat. Nanotechnol. **8**, 899 (2013).

[26] T. Kurumaji, T. Nakajima, M. Hirschberger, A. Kikkawa, Y. Yamasaki, H. Sagayama, H. Nakao, Y. Taguchi, T.-H. Arima, and Y. Tokura, Skyrmion lattice with a giant topological Hall effect in a frustrated triangular-lattice magnet, Science **365**, 914 (2019).

[27] H. Chen, Q. Niu, and A. H. MacDonald, Anomalous Hall effect arising from noncollinear antiferromagnetism, Phys. Rev. Lett. **112**, 017205 (2014).

[28] S.-S. Zhang, H. Ishizuka, H. Zhang, G. B. Halász, and C. D. Batista, Real-space Berry curvature of itinerant electron systems with spin-orbit interaction, Phys. Rev. B **101**, 024420 (2020).

[29] J. M. Luttinger, Quantum theory of cyclotron resonance in semiconductors: General theory, Phys. Rev. **102**, 1030 (1956).

[30] D. Zhang, H. Wang, J. Ruan, G. Yao, and H. Zhang, Engineering topological phases in the Luttinger semimetal α-Sn, Phys. Rev. B **97**, 195139 (2018).

[31] E.-G. Moon, C. Xu, Y. B. Kim, and L. Balents, Non-Fermi-liquid and topological states with strong spin-orbit coupling, Phys. Rev. Lett. **111**, 206401 (2013).

[32] J.-W. Rhim and Y. B. Kim, Quantum oscillations in the Luttinger model with quadratic band touching: Applications to pyrochlore iridates, Phys. Rev. B **91**, 115124 (2015).

[33] J. Smit, The spontaneous Hall effect in ferromagnetics I, Physica **21**, 877 (1955).

[34] J. Kondo, Anomalous Hall effect and magnetoresistance of ferromagnetic metals, Prog. Theor. Phys. **27**, 772 (1962).

[35] A. A. Belavin and A. M. Polyakov, Metastable states of two-dimensional isotropic ferromagnets, Pis'ma. Zh. Eksp. Teor. Fiz. **22**, 503 (1975) [JETP Lett. **22**, 245 (1975)].

[36] S. Mühlbauer, B. Binz, F. Jonietz, C. Pfleiderer, A. Rosch, A. Neubauer, R. Georgii, and P. Böni, Skyrmion lattice in a chiral magnet, Science **323**, 5916 (2009).

[37] X. Z. Yu, N. Kanazawa, Y. Onose, K. Kimoto, W. Z. Zhang, S. Ishiwata, Y. Matsui, and Y. Tokura, Near room-temperature formation of a skyrmion crystal in thin-films of the helimagnet FeGe, Nat. Mater. **10**, 106 (2011).

[38] I. Kézsmárki, S. Bordács, P. Milde, E. Neuber, L. M. Eng, J. S. White, H. M. Rønnow, C. D. Dewhurst, M. Mochizuki, K. Yanai, H. Nakamura, D. Ehlers, V. Tsurkan, and A. Loidl, Néel-type skyrmion lattice with confined orientation in the polar magnetic semiconductor GaV_4S_8, Nat. Mater. **14**, 1116 (2015).

[39] Y. Tokura and N. Kanazawa, Magnetic skyrmion materials, Chem. Rev. **121**, 2857 (2021).

[40] R. Saha, H. L. Meyerheim, B. Göbel, B. K. Hazra, H. Deniz, K. Mohseni, V. Antonov, A. Ernst, D. Knyazev, A. Bedoya-Pinto, I. Mertig, and S. S. P. Parkin, Observation of Néel-type skyrmions in acentric self-intercalated $Cr_{1+\delta}Te_2$, Nat. Commun. **13**, 3965 (2022).

[41] T. Nagase, Y.-G. So, H. Yasui, T. Ishida, H. K. Yoshida, Y. Tanaka, K. Saitoh, N. Ikarashi, Y. Kawaguchi, M. Kuwahara, and M. Nagao, Observation of domain wall bimerons in chiral magnets, Nat. Commun. **12**, 3490 (2021).

[42] J. M. Luttinger and W. Kohn, Motion of electrons and holes in perturbed periodic fields, Phys. Rev. **97**, 869 (1955).

[43] C. Luo, K. Chen, V. Ukleev, S. Wintz, M. Weigand, R.-M. Abrudan, K. Prokeš, and F. Radu, Direct observation of Néel-type skyrmions and domain walls in a ferrimagnetic $DyCo_3$ thin film, Commun. Phys. **6**, 218 (2023).